Electronic Supplementary Material (ESI) for Lab on a Chip.

Supporting Information:

Supplemental Figures:

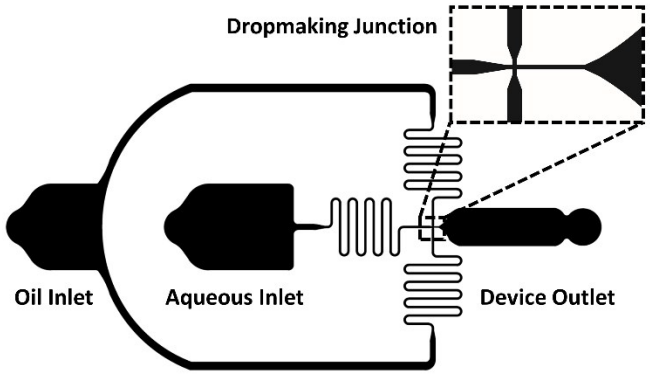

Figure S1: Design for the droplet microfluidic beadmaking device. Junction dimensions were approximately 7 µm x 7 µm with a height of 10 µm. Stable dropmaking was achieved in the dripping regime. The device widens rapidly downstream of the junction to reduce the shear force on the droplets.

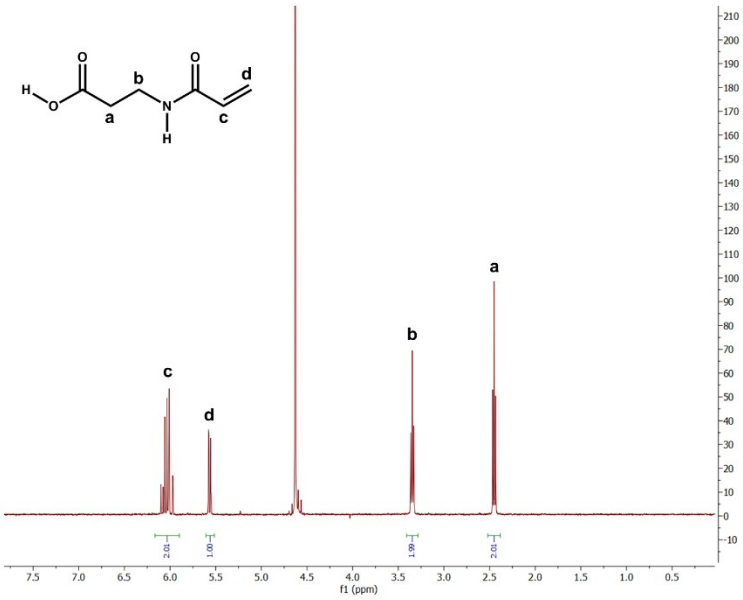

Figure S2: ^{1}H NMR spectrum collected on a Varian Inova 400 used to confirm the synthesis of Acryloyl-β-alanine.

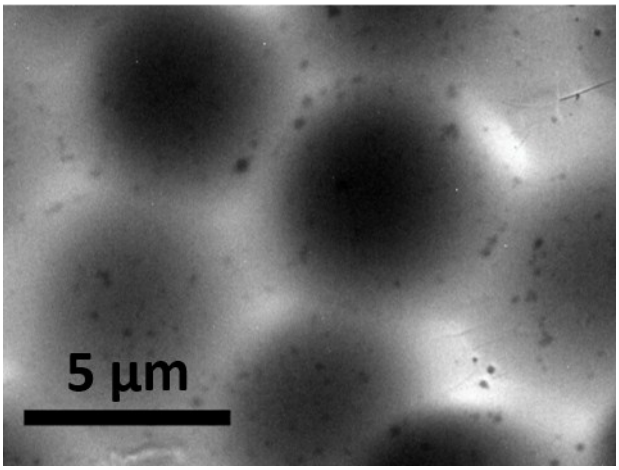

Figure S3: TEM image of dried MHB1. Dark spots distributed throughout gels correspond to magnetic nanoparticles trapped inside the hydrogels.

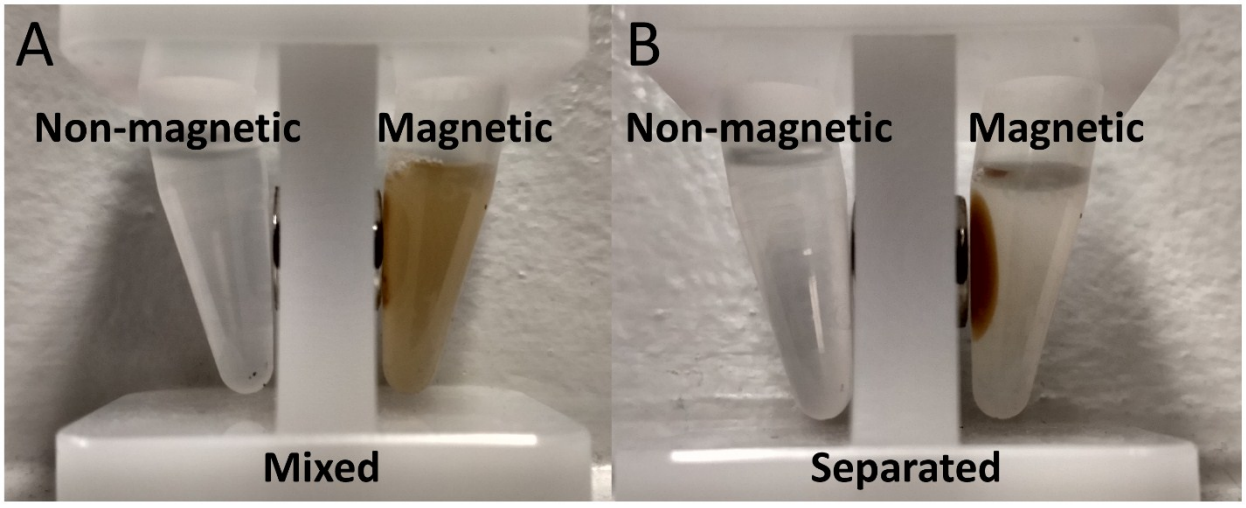

Figure S4: A) Well mixed suspensions of hydrogel beads produced without (left tube) and with (right tube) magnetic nanoparticles trapped inside the gels. B) Within minutes the magnetic gels are pulled towards the magnet and are separated from the solution. The non-magnetic gels remain in suspension.

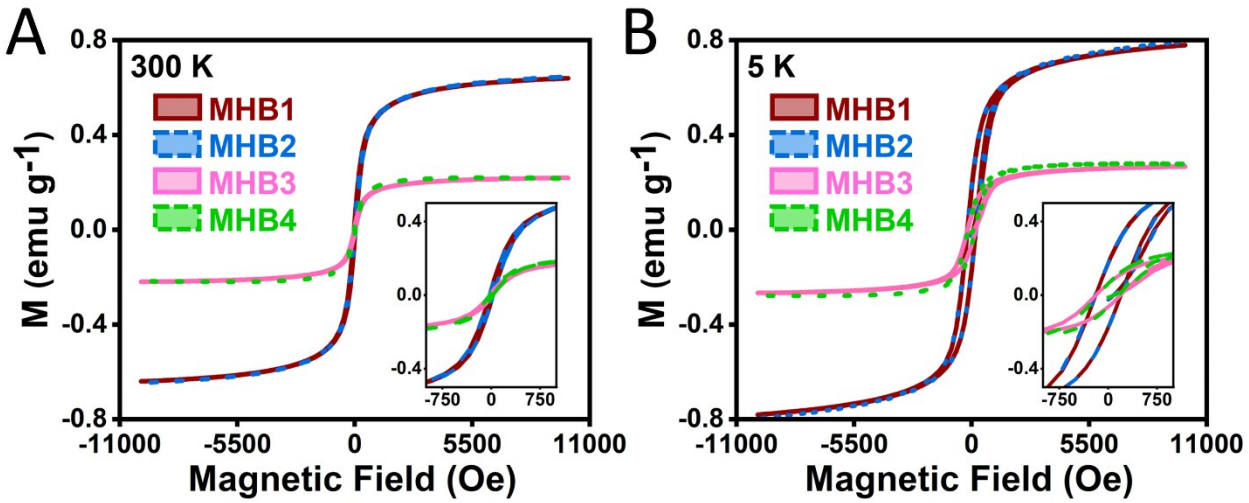

Figure S5: A) SQUID Magnetometer plots for each bead type collected at B) 300 K and at C) 5 K. The observed behavior confirms that the hydrogel beads are rendered magnetic by the incorporation of the nanoparticles.

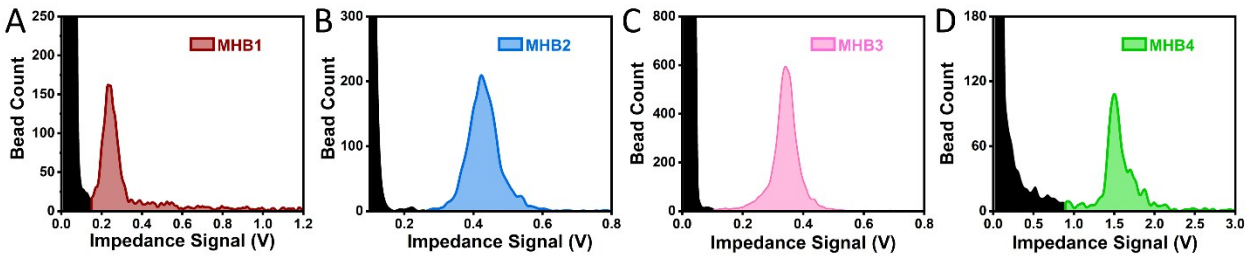

Figure S6: Histograms of the different bead populations showing the counts binned by voltage. A) MHB1 B) MHB2 C) MHB3 D) MHB4. The impedance signals of MHB2 and MHB3 are overlapped since the effects of the increase in density are counteracted by the reduction in bead volume.

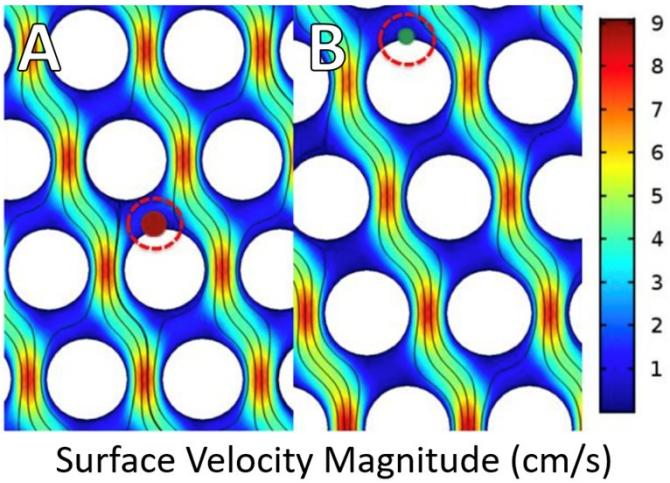

Figure S7: COMSOL simulations of the magnitude of the surface velocity inside the capture chamber; streamlines are also indicated. The green and red particles have diameters of 8 and 13 µm respectively. These results show location of low velocity regions present behind the pillars. These regions have the highest likelihood of nonspecific capture. Since beads of different sizes experience the flow profile differently, size variations impact the rates of nonspecific capture.

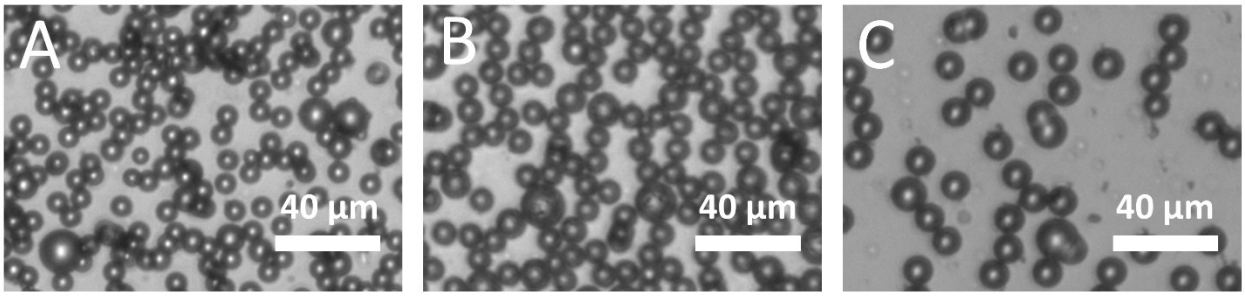

Figure S8: Widefield microscope images of solid magnetic beads; A) 6-8 µm particles, B) 8-10 µm particles, C) 10-14 µm particles. Large particles can be seen across all bead types.

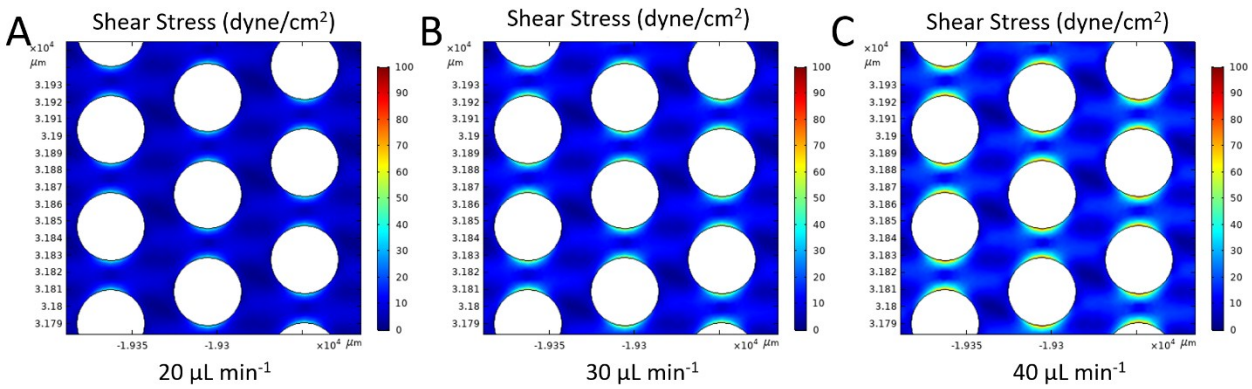

Figure S9: COMSOL simulations of the shear stress inside the capture chamber of the device at different flow rates. Redder areas indicate higher shear stress, while bluer regions have lower shear stress. As the flow rate increases the shear stress at the pillars increases decreasing the likelihood of bead capture.

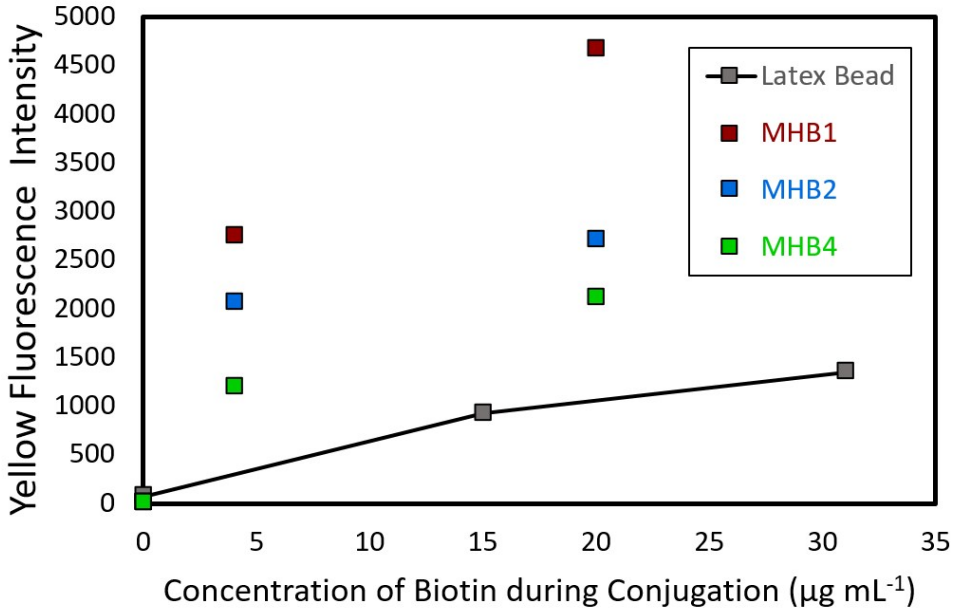

Figure S10: Flow cytometry measurements comparing the efficiency of surface functionalization between MHBs and commercially available latex beads. Since the MHBs have higher surface functional group density, they produce a larger fluorescent response relative to the concentration of biotin during functionalization.

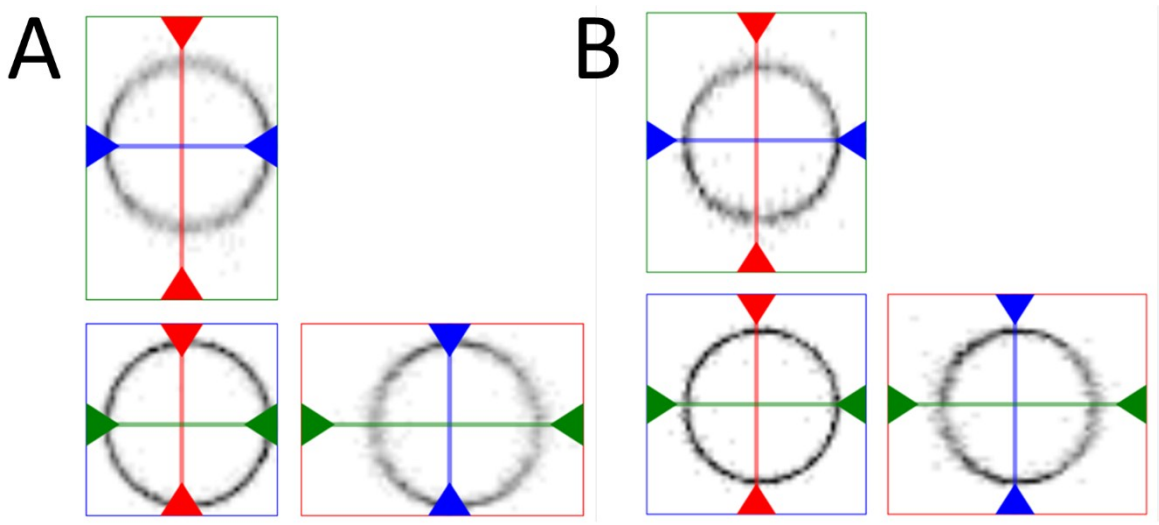

Figure S11: Confocal images of A) MHB2 and B) MHB4 after conjugation to biotin and fluorescent labeling by streptavidin binding.

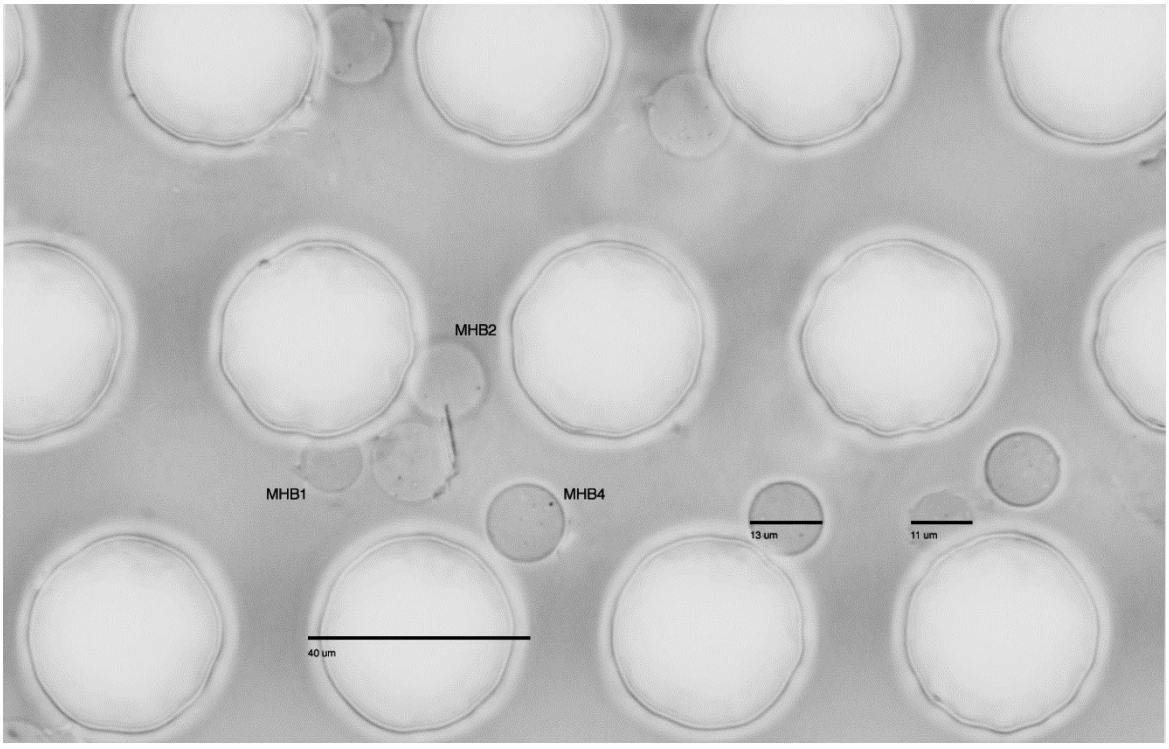

Figure S12: Image showing various MHBs captured to pillars inside the capture chamber of the device

Supplementary Data:

Supplementary Data: ^{1}H NMR spectrum collected on a Varian Inova 400 used to confirm the synthesis of Acryloyl-β-alanine.

Estimation of Magnetic Nanoparticle Loading: The saturation magnetization (M_s) of each sample was measured and used to estimate the number of magnetic nanoparticles per microsphere. According to the manufacturer, the nanoparticles consist of at least 80% γ-Fe_2O_3 which has a bulk M_s of 76 emu g^{-1}. We assumed that the magnetic particles were uniformly incorporated and did not significantly alter the density of bulk hydrogel. As such we could use the hydrogel diameter, the nanoparticle diameter, and the dry mass of the sample to estimate the number of nanoparticles per microsphere. Accordingly, MHB1 and 3 contained on average 20 magnetic nanoparticles per microspheres while MHB2 and MHB4 contained 23 nanoparticles. This result is consistent with a Poisson loading.

Sequences used for DNA detection:
TP53:
Capture Oligo: 5'-GGCAGCGCCTCACAAC-TTTTTTTTT-Amine-3'
Gene Fragment: 5'-GTTGTGAGGCGCTGCCCCCACCATGAGCGCTGCTCAGATAGCGATG-3'
Detection Oligo: 5'-Biotin-TTTTTTTTT-CATCGCTATCTGAGCAGCG-3'

PIK3CA:
Capture Oligo: 5'-AGAAAATCTTTCTCCTGCTCAGTG-TTTTTTTTT-Amine-3'
Gene Fragment: 5'-CACTGAGCAGGAGAAAGATTTTCTATGGAGTCACAGGTAAGTGCTAAAATGGA-3'
Detection Oligo: 5'-Biotin-TTTTTTTTT-TCCATTTTAGCACTTACCTGT-3'

Supplementary Video 1: MHB Captured by Streptavidin-Coated Pillar

AUTHOR INFORMATION

Corresponding Author

hshan@illinois.edu

ORCID

Thomas W. Cowell: 0000-0002-7463-9339
Enrique Valera: 0000-0003-1359-66190
Joonhyuck Park: 0000-0003-1509-724X
Jacob Berger: 0000-0002-5429-3940
Rashid Bashir: 000-0002-7225-9180
Hee-Sun Han: 0000-0003-3616-291X

Author Contributions

T.W.C., E.V., R.B., and H.-S.H. have conceived of the idea and designed experiments. T.W.C, J.P., and R.D. designed and synthesized beads. T.W.C, performed magnetic characterization of the beads. T.W.C., J.P. and A.W.S. performed imaging experiments. T.W.C, E.V., and A.J. functionalized beads and conducted binding assays. E.V. and A.J. performed electrical characterization of the beads. A.J. and E.V. performed the capture experiments. J.B. worked on the fabrication of the electrodes. T.W.C., E.V., R.B., and H.-S.H prepared the manuscript.